P Selected for a Viewpoint in *Physics*
PHYSICAL REVIEW LETTERS

℘

Coherent Ultrafast Measurement of Time-Bin Encoded Photons

John M. Donohue,* Megan Agnew, Jonathan Lavoie, and Kevin J. Resch

*Institute for Quantum Computing and Department of Physics & Astronomy, University of Waterloo,
Waterloo, Ontario N2L 3G1, Canada*

Time-bin encoding is a robust form of optical quantum information, especially for transmission in optical fibers. To readout the information, the separation of the time bins must be larger than the detector time resolution, typically on the order of nanoseconds for photon counters. In the present work, we demonstrate a technique using a nonlinear interaction between chirped entangled time-bin photons and shaped laser pulses to perform projective measurements on arbitrary time-bin states with picosecond-scale separations. We demonstrate a tomographically complete set of time-bin qubit projective measurements and show the fidelity of operations is sufficiently high to violate the Clauser-Horne-Shimony-Holt-Bell inequality by more than 6 standard deviations.

Qubits encoded in the time-bin degree of freedom are particularly well suited for long-distance quantum communication and fundamental experiments [1–6]. Time-bin states can be prepared using an unbalanced interferometer [7,8], where photons may take a short path and arrive early ($|e\rangle$) or a long one and arrive late ($|\ell\rangle$) with a time difference $\tau_{e\ell}$ greater than the photon coherence time. Measurements of time-bin states are typically performed with an identical interferometer [see Fig. 1(a)]. However, high-fidelity measurements require that $\tau_{e\ell}$ be greater than the detector time resolution, which is typically much longer than the coherence time. Experimentally, delays on the order of nanoseconds have been used [3,6]; recent advances in photon counting technology could conceivably reduce this delay to 30 ps [9]. Even faster detectors would improve time-bin encodings, allowing a higher information density while reducing the demands on interferometric stabilization.

Ultrafast laser pulses and nonlinear optics provide a framework for single-photon measurement on timescales much faster than electronics [10,11]. A promising coherent nonlinear effect for single-photon ultrafast measurements is sum-frequency generation (SFG), a process in which two pulses interact in a nonlinear material to produce a third with frequency equal to the sum of the inputs [12–15]. SFG in conjunction with pulse-shaping techniques is a powerful tool for manipulating single-photon temporal waveforms [16–18].

In the present work, we show how sum-frequency generation and pulse shaping enable coherent measurements of time-bin states with a temporal separation on the picosecond timescale. To explicitly demonstrate the coherent aspects of our technique, we perform a tomographically complete set of measurements on an entangled time-bin state for state reconstruction [19–21]. Furthermore, we show that our measurement proceeds with sufficiently high fidelity to convincingly violate the Clauser-Horne-Shimony-Holt(CHSH)-Bell inequality [22,23].

The principle of our measurement scheme is based on SFG with oppositely chirped pulses. A chirped pulse is stretched such that its instantaneous frequency varies linearly in time. By combining two oppositely chirped pulses through SFG, the bandwidth of the resulting pulse is drastically narrowed. Additionally, by delaying one of the pulses, the central frequency of the generated light changes by an amount proportional to the delay. This has been shown for laser pulses [24,25] and a single photon with a strong laser pulse [18]. If a pulse (or photon) is in a superposition of
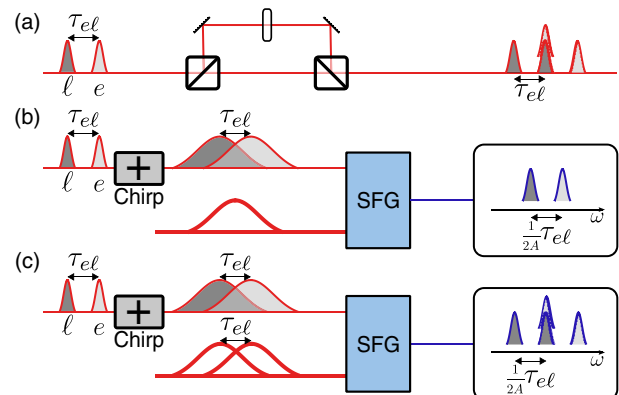

FIG. 1 (color online).   Measuring time-bin qubits. (a) In typical time-bin measurement schemes, an input time-bin state is sent through an unbalanced interferometer matched to the bin separation. High-fidelity measurement requires isolating the middle output pulse, necessitating a large delay $\tau_{e\ell}$. (b) A photon encoding a time-bin qubit is chirped and undergoes SFG with an equal and oppositely chirped strong laser pulse. The SFG contains two peaks separated in frequency by an amount proportional to the time delay, $\tau_{e\ell}$. (c) If the chirped strong laser pulse is itself in a superposition of two time bins, the output spectrum contains three peaks. In this case, high-fidelity measurement requires isolating the middle frequency. The process is directly analogous to conventional time-bin measurement, with the signal converted from time to frequency.

153602-1

two time bins, it will exit the process in a superposition of two frequencies [see Fig. 1(b)]. The process is thus a coherent interface between time and frequency. If *both* inputs are in superpositions of time bins with the same separation, the spectrum of the SFG output is analogous to the temporal profile of interferometric time-bin measurement, with three distinct frequencies. The middle peak results from the interference of two contributions, with an intensity proportional to the probability expected for a controllable projective measurement [see Fig. 1(c)].

We model our scheme by expressing the electric field of a chirped laser pulse as $E(\omega; \tau, A) = f(\omega)e^{i\omega\tau}e^{iA(\omega - \omega_0)^2}$, where τ is a time delay, A characterizes the chirp strength, and $f(\omega) \propto \exp[-(\omega - \omega_0)^2/(4\sigma^2)]$ is the spectral amplitude. We define a single photon in the early time bin as $|e\rangle \propto \int d\omega E(\omega; 0, 0)\hat{a}_\omega^\dagger|0\rangle$ and one in the late time bin as $|\ell\rangle \propto \int d\omega E(\omega; \tau_{e\ell}, 0)\hat{a}_\omega^\dagger|0\rangle$. A time-bin qubit can be written as $|\psi\rangle \approx \cos\theta|e\rangle + e^{i\phi}\sin\theta|\ell\rangle$. We can similarly define a superposition of two strong laser pulses separated in time by $\tau_{e\ell}$ as

$$E_\Lambda(\omega, \alpha, \beta) = \cos\alpha E(\omega; 0, 0) + e^{i\beta}\sin\alpha E(\omega; \tau_{e\ell}, 0), \quad (1)$$

where α and β determine the relative amplitude and phase, respectively.

A strong laser pulse and a single photon with equal and opposite large chirps ($A^2\sigma^4 \gg 1$) produce narrow band SFG with a central frequency that depends on their relative time delay [18]. The SFG bandwidth is $\sigma_3 \leq 1/(2\sqrt{2}A\sigma)$, where σ is the smaller of the two input bandwidths. Now consider SFG between a positively chirped time-bin qubit and a negatively chirped version of the classical pulse from Eq. (1). For the two contributions to the SFG from the single photon and strong laser pulse being both early or both late, the up-converted photon will be spectrally narrow with a central frequency ω_M equal to the sum of the input central frequencies. Another contribution arises from the single photon arriving early and the strong laser pulse late, which is blueshifted to $\omega_B = \omega_M + \tau_{e\ell}/2A$. Similarly, if the arrival order is reversed, the contribution is redshifted to $\omega_R = \omega_M - \tau_{e\ell}/2A$. To spectrally separate the three components, we require $\tau_{e\ell} \gg 1/\sigma$. Additionally, if $\tau_{e\ell} \ll 1/\sigma_3$ or equivalently $\tau_{e\ell} \ll A\sigma$, the SFG at ω_M exhibits interference with an intensity of $I_M \propto |\cos\theta\cos\alpha + e^{i(\phi+\beta)}\sin\theta\sin\alpha|^2$. This is proportional to $|\langle\Lambda|\psi\rangle|^2$, which is the success probability of a projective measurement onto the state $|\Lambda\rangle = \cos\alpha|e\rangle + e^{-i\beta}\sin\alpha|\ell\rangle$, where $|\Lambda\rangle$ is controlled by the shape of the laser pulse from Eq. (1). This technique extends naturally to time-bin qudits of arbitrary dimension. See the Supplemental Material for more details [26].

Our setup is shown in Fig. 2. A pulsed Ti:sapphire laser (repetition rate 80 MHz, average power 2.4 W) centered at 790.2 nm with bandwidth 11.8 nm (FWHM) produces 0.8 W centered at 393.8 nm with a bandwidth of 1.2 nm through second-harmonic generation (SHG) in bismuth
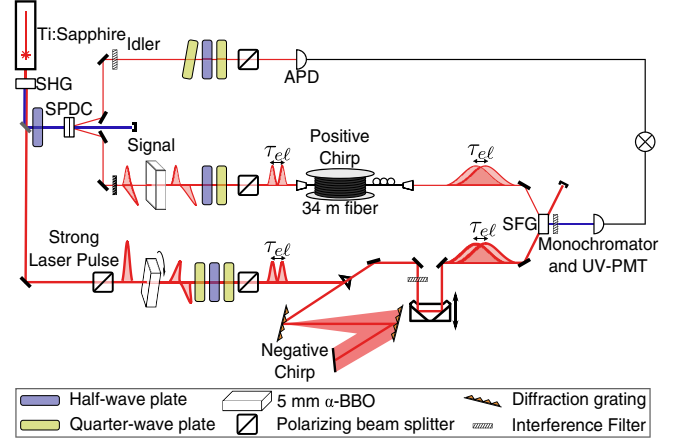

FIG. 2 (color online). Experimental setup. Polarization-entangled photon pairs (signal and idler) are generated via down-conversion (SPDC) in orthogonally oriented nonlinear crystals (extra crystals used for compensation not shown). The signal photon is converted to a time-bin qubit using a birefringent crystal (5 mm α-BBO) and polarizer. The signal acquires a positive chirp in 34 m of optical fiber. The strong laser pulse is prepared using an identical birefringent crystal and a series of wave plates to set the phase, then negatively chirped using gratings. The photon and laser pulse are combined in a nonlinear crystal to produce SFG. The middle frequency is detected using a photon counter after a monochromator.

borate (BiBO). The UV beam is rotated to diagonal polarization before passing through two orthogonally oriented β-barium borate (BBO) crystals to produce photon pairs via type-I down-conversion (SPDC) in the polarization state $|\Phi^+\rangle = (1/\sqrt{2})(|HH\rangle + |VV\rangle)$ [27], where $|H\rangle$ and $|V\rangle$ are horizontal and vertical polarizations, respectively. To compensate walk-off, we inserted 1 mm of α-BBO into the UV beam path and 1 mm of BiBO with a cut angle of 152.6° into the signal arm [28]. The signal is filtered to 810.4 nm with bandwidth 4.53 ± 0.09 nm FWHM, and the idler to 767.1 nm with bandwidth 2.37 ± 0.02 nm. We directly detect the signal and idler photons using avalanche photodiodes (APD, Perkin-Elmer SPCM-AQ4C). Summing the coincidence rates over all H/V combinations yields a total of 135 kHz.

We convert the signal photon from polarization to time-bin encoding by inserting 5 mm of α-BBO cut at 90° into the signal arm such that $|H\rangle$ is aligned with the extraordinary (fast) axis and project onto diagonal polarization with a polarizing beam splitter to erase polarization information, leaving the state $|\tilde{\Phi}^+\rangle = (1/\sqrt{2})(|He\rangle + |V\ell\rangle)$. The α-BBO introduces a relative group delay of $\tau_{e\ell} = 2.16 \pm 0.03$ ps between the polarization components, measured through chirped-pulse interferometry [29]. This delay is greater than the photon coherence time, $1/\sigma = 0.362$ ps, fulfilling the requirements for distinct time bins.

A strong laser pulse with field $E_\Lambda(\omega, \alpha, \beta)$ is prepared by sending the remaining fundamental through another 5-mm α-BBO crystal, where rotation about the beam

axis controls α, the relative weighting of early and late components. We can control the phase β between the components through the rotation of a half-wave plate between two quarter-wave plates set to 0°. Polarization information is then removed using another polarizing beam splitter. The phase β is 4 times the half-wave plate angle, with an offset due to the birefringence in the system. This sequence simplifies projections onto the standard states: $|e\rangle$, $|\ell\rangle$, and $(1/\sqrt{2})(|e\rangle + e^{i\phi}|\ell\rangle)$ with $\phi = \{-\pi/2, 0, \pi/2, \pi\}$. To extend to arbitrary projections, the rotatable α-BBO may be replaced by a rotatable half-wave plate and an α-BBO set at 45 deg.

The positive chirp of $A = (670 \pm 1) \times 10^3$ fs^2 is applied to the single photons by passing through 34 m of single-mode fiber. The opposite chirp on the strong laser pulse is applied using gratings [30]. The strong laser beam is then filtered to 785.7 nm with a bandwidth of 11.9 ± 0.3 nm and passed through a delay line, with average power 146 mW output. The two pulses are focused on a 1-mm BiBO crystal phase matched for type-I SFG producing a UV signal detectable by a photon counter (UV-PMT, Hamamatsu H10682-210).

The resulting signal is sent to a fiber-coupled spectrometer (Princeton Instruments Acton Advanced SP2750A), which we use as either a monochromator for photon counting or a full spectrometer. With β set to 0, the up-converted signal spectrum, averaged over five 90 min runs, is seen in Fig. 3 and exhibits three distinct peaks. The middle peak, centered at 399.82 nm, has a bandwidth of 0.043 ± 0.002 nm. This is in reasonable agreement with the prediction of 0.035 ± 0.002 nm from the expected bandwidth corrected for our 0.03-nm spectrometer resolution [18]. The side peaks are centered at 399.68 and 399.96 nm. The average separation from the main peak $\Delta\lambda_{\mathrm{expt}} = 0.138 \pm 0.003$ nm agrees with the prediction $\Delta\lambda_{\mathrm{th}} = 0.137 \pm 0.002$ nm calculated from the measured chirp and α-BBO

birefringence. The separation is sufficiently large compared to the linewidth, enabling effective filtering of the side peaks with a monochromator window of 0.11 nm, with a transmission efficiency of 6% in our implementation.

After entangled state preparation, we vary the phase β of the laser pulse and record coincidences between the UV-PMT and idler APD when the idler polarization is measured as $|D\rangle = (1/\sqrt{2})(|H\rangle + |V\rangle)$. We repeat this process for idler measurements of $|A\rangle = (1/\sqrt{2})(|H\rangle - |V\rangle)$, $|L\rangle = (1/\sqrt{2})(|H\rangle + i|V\rangle)$, and $|R\rangle = (1/\sqrt{2})(|H\rangle - i|V\rangle)$ (Fig. 4). The rate of coincidence counts summed over each basis was 1 Hz, from which an internal up-conversion efficiency of 0.06% was found by accounting for the losses due to fiber, filtering, and removal of polarization information. Rates of single-photon detection events were also recorded (see Supplemental Material [26]). The coincidences oscillate sinusoidally with an average visibility among the four curves of $89.3 \pm 1.7\%$. A subset of these data, for phases indicated by vertical lines in Fig. 4, is sufficient to test the CHSH-Bell inequality [22,23], written as $S = E(a, b) + E(a, b') + E(a', b) - E(a', b') \leq 2$, where $E(a, b)$ is the correlation and $\{a, a', b, b'\}$ are measurement settings. This inequality holds for local hidden-variable models but can be violated by entangled quantum states. We measure polarization states of the form $(1/\sqrt{2})(|H\rangle \pm e^{i\xi}|V\rangle)$ and time-bin states of the form $(1/\sqrt{2})(|e\rangle \pm e^{i\zeta}|\ell\rangle)$, where the "+" and "−" outcomes are assigned values $+1$ and -1, respectively.
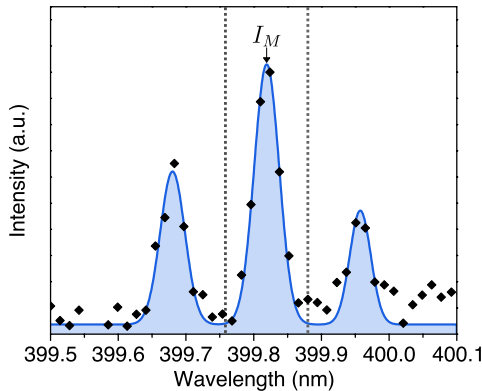

FIG. 3 (color online). Sum-frequency spectrum, in arbitrary units (a.u.). The up-converted signal spectrum (background subtracted) taken using our spectrometer, with β set to 0. A fit to the data is shown in blue. The monochromator selected those wavelengths that fall between the dotted lines.
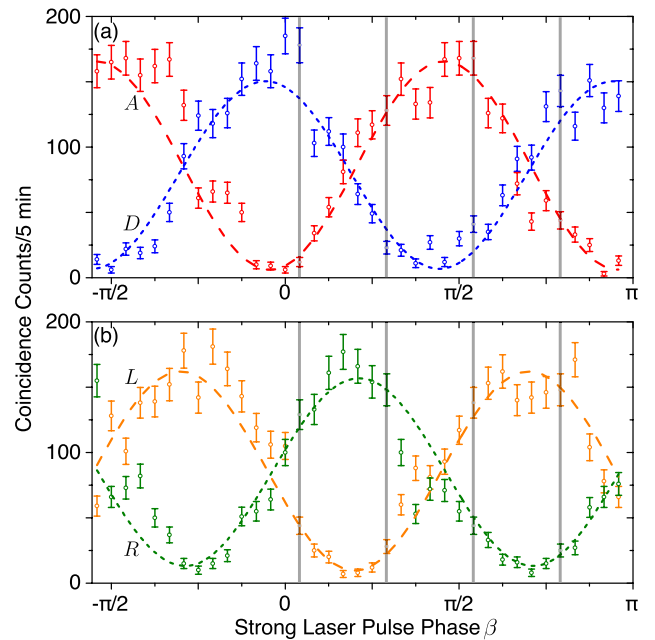

FIG. 4 (color online). Coincidence counts versus β. The idler is projected into the diagonal basis in (a) ($|D\rangle$ in blue and $|A\rangle$ in red) and the circular basis in (b) ($|L\rangle$ in orange and $|R\rangle$ in green). The CHSH-Bell inequality was violated using the data points indicated by the gray lines with a value $S = 2.54 \pm 0.08$.

Choosing $\xi_a = 0$, $\xi_{a'} = \pi/4$, $\zeta_b = 0.066\pi$, and $\zeta_{b'} = 0.316\pi$, the CHSH-Bell parameter was found to be $S = 2.54 \pm 0.08$, corresponding to a violation of the inequality by 6.8 standard deviations.

We fixed the phase of the laser pulse to $\beta = 0$ and used the monochromator to select frequencies corresponding to the peaks in Fig. 3. We measured the coincidence counts between the idler for polarization measurements $\{H, V, D, A, R, L\}$ and the UV-PMT when the monochromator was centered on each peak. The coincidence counts for each setting and bin are shown in Fig. 5(a), showing high contrast in the middle bin. Continuing this approach for different settings of α and β, we performed two-qubit tomography on our time-bin-encoded signal and polarization-encoded idler using an overcomplete set of 36 measurements [19] and iterative maximum-likelihood reconstruction [31]. Tomography on the initial polarization state, shown in Fig. 5(b), yielded a fidelity of $94.01 \pm 0.02\%$ with the Bell state $|\Phi^+\rangle$. The final state was measured with an integration time of 15 min per setting after up-conversion and spectral filtering. The fidelity of the output state with the state $|\tilde{\Phi}^+\rangle$ was found to be $89.4 \pm 0.7\%$, and the fidelity with the reconstructed density matrix of the initial

polarization state was found to be $95.0 \pm 0.8\%$ [Fig. 5(c)]. Thus, our chirped-pulse up-conversion technique was able to retrieve the correlations through quantum state tomography with minimal loss of fidelity.

We have demonstrated ultrafast time-bin measurements using chirped-pulse up-conversion as a coherent time-to-frequency interface. We showed the control necessary to perform quantum state tomography on time-bin entangled states and sufficiently high fidelity to convincingly violate the CHSH-Bell inequality. This technique operates at the fundamental limit for time-bin states where the coherence time of the light, not the time resolution of the detector, constrains the bin separation. Future work will focus on improving the efficiency of our scheme. With the use of periodically poled materials, nearly perfect single-photon up-conversion efficiency has been achieved [13,32]; combining such materials with cavities has been shown to significantly improve efficiencies for weak fields or biphotons [33]. High-transmission filters [34] or restrictive phase-matching conditions may be used to increase the filtering efficiency. At higher efficiencies, this scheme may be extended to time-bin qudits, increasing the information density of time-bin encodings.
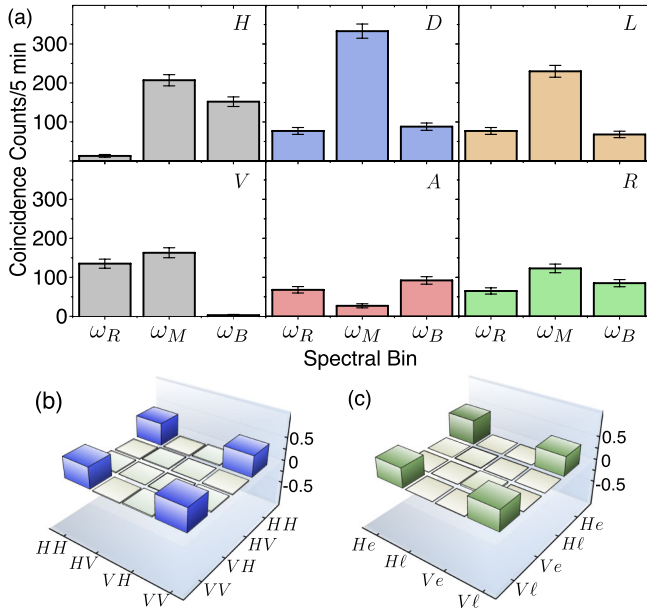
FIG. 5 (color online). Quantum state reconstruction. (a) Coincidence counts between the idler and the SFG photon in each peak from Fig. 3, for $\beta = 0$ and the indicated polarization measurement of the idler. (b) Real part of the reconstructed density matrix of the initial two-photon polarization state produced from the SPDC source, which has a fidelity of 94% with $|\Phi^+\rangle$. (c) Real part of the reconstructed density matrix of the time-bin-encoded signal and polarization-encoded idler using chirped-pulse up-conversion to measure the time-bin states; the state has 95% fidelity with the reconstructed density matrix of the initial state. Imaginary parts of both matrices were negligibly small and are in the Supplemental Material [26].

*jdonohue@uwaterloo.ca

[1] W. Tittel, J. Brendel, H. Zbinden, and N. Gisin, Phys. Rev. Lett. **81**, 3563 (1998).
[2] J. Brendel, N. Gisin, W. Tittel, and H. Zbinden, Phys. Rev. Lett. **82**, 2594 (1999).
[3] W. Tittel, J. Brendel, H. Zbinden, and N. Gisin, Phys. Rev. Lett. **84**, 4737 (2000).
[4] I. Marcikic, H. de Riedmatten, W. Tittel, V. Scarani, H. Zbinden, and N. Gisin, Phys. Rev. A **66**, 062308 (2002).
[5] I. Marcikic, H. de Riedmatten, W. Tittel, H. Zbinden, M. Legré, and N. Gisin, Phys. Rev. Lett. **93**, 180502 (2004).
[6] A. Martin, F. Kaiser, A. Vernier, A. Beveratos, V. Scarani, and S. Tanzilli, Phys. Rev. A **87**, 020301 (2013).
[7] J. D. Franson, Phys. Rev. Lett. **62**, 2205 (1989).
[8] J. D. Franson, Phys. Rev. A **44**, 4552 (1991).
[9] R. Hadfield, Nat. Photonics **3**, 696 (2009).
[10] J. Shah, IEEE J. Quantum Electron. **24**, 276 (1988).
[11] B. Dayan, A. Pe'er, A. A. Friesem, and Y. Silberberg, Phys. Rev. Lett. **93**, 023005 (2004).
[12] J. Huang and P. Kumar, Phys. Rev. Lett. **68**, 2153 (1992).
[13] A. P. VanDevender and P. G. Kwiat, J. Mod. Opt. **51**, 1433 (2004).
[14] S. Tanzilli, W. Tittel, M. Halder, O. Alibart, P. Baldi, N. Gisin, and H. Zbinden, Nature (London) **437**, 116 (2005).
[15] S. Ramelow, A. Fedrizzi, A. Poppe, N. K. Langford, and A. Zeilinger, Phys. Rev. A **85**, 013845 (2012).
[16] D. Kielpinski, J. F. Corney, and H. M. Wiseman, Phys. Rev. Lett. **106**, 130501 (2011).

[17] A. Eckstein, B. Brecht, and C. Silberhorn, Opt. Express **19**, 13 770 (2011).

[18] J. Lavoie, J. M. Donohue, L. G. Wright, A. Fedrizzi, and K. J. Resch, Nat. Photonics **7**, 363 (2013).

[19] M. D. de Burgh, N. K. Langford, A. C. Doherty, and A. Gilchrist, Phys. Rev. A **78**, 052122 (2008).

[20] H. Takesue and Y. Noguchi, Opt. Express **17**, 10 976 (2009).

[21] S. X. Wang, C. Chan, P. Moraw, D. R. Reilly, J. B. Altepeter, and G. S. Kanter, Phys. Rev. A **86**, 042122 (2012).

[22] J. Bell, Physics **1**, 195 (1964).

[23] J. Clauser, M. Horne, A. Shimony, and R. Holt, Phys. Rev. Lett. **23**, 880 (1969).

[24] F. Raoult, A C. L. Boscheron, D. Husson, C. Sauteret, A. Modena, V. Malka, F. Dorchies, and A. Migus, Opt. Lett. **23**, 1117 (1998).

[25] K. Osvay and I. N. Ross, Opt. Commun. **166**, 113 (1999).

[26] See Supplemental Material at http://link.aps.org/supplemental/10.1103/PhysRevLett.111.153602 for a complete derivation from theory, extension to time-bin qudits, and additional data.

[27] P. G. Kwiat, E. Waks, A. G. White, I. Appelbaum, and P. H. Eberhard, Phys. Rev. A **60**, R773 (1999).

[28] J. Lavoie, R. Kaltenbaek, and K. J. Resch, New J. Phys. **11**, 073051 (2009).

[29] M. D. Mazurek, K. M. Schreiter, R. Prevedel, R. Kaltenbaek, and K. J. Resch, Sci. Rep. **3**, 1582 (2013).

[30] E. Treacy, IEEE J. Quantum Electron. **5**, 454 (1969).

[31] M. Ježek, J. Fiurášek, and Z. Hradil, Phys. Rev. A **68**, 012305 (2003).

[32] R. T. Thew, H. Zbinden, and N. Gisin, Appl. Phys. Lett. **93**, 071104 (2008).

[33] S. Sensarn, I. Ali-Khan, G. Y. Yin, and S. E. Harris, Phys. Rev. Lett. **102**, 053602 (2009).

[34] P. S. Kuo, J. S. Pelc, O. Slattery, Y.-S. Kim, M. M. Fejer, and X. Tang, Opt. Lett. **38**, 1310 (2013).